Journal of King Saud University – Science 31 (2019) 849–858

Contents lists available at ScienceDirect

Journal of King Saud University – Science

journal homepage: www.sciencedirect.com

Original article

Utilization of salt activated *Raphia hookeri* seeds as biosorbent for Erythrosine B dye removal: Kinetics and thermodynamics studies

C.C. Okoye *, O.D. Onukwuli, C.F. Okey-Onyesolu

Department of Chemical Engineering, Nnamdi Azikiwe University, PMB 5025, Awka, Anambra State, Nigeria

ARTICLE INFO

Article history:
Received 12 September 2017
Accepted 26 November 2017
Available online 5 December 2017

ABSTRACT

The use of a non-conventional precursor, Raphia hookeri seeds, (RHS) for the production of activated carbon through thermal and salt activation for the adsorption of Erythrosine B (EB) dye in an aqueous solution was investigated. The physicochemical properties of the prepared activated carbon were studied using standard methods. Scanning electron microscopy (SEM) displayed the surface morphology micrograph and Fourier Transform Infrared was used to identify the functional groups of the activated carbon. Adsorptive performance tests at various temperatures were evaluated at optimum results of 75 μm adsorbent particle size, 1 g adsorbent dosage, 100 mg/L adsorbate concentration and pH 4. An equilibration time of 90 minutes is sufficient at 30 °C for 87.78% adsorption of EB on SARHS. Experimental data were fitted into non-linearized pseudo-first order (PFO) and pseudo-second order (PSO) kinetic models. PSO better fitted the experimental data based on SSE (%), RMS and R^2 results. Computations from intra-particle diffusion kinetic model reveal that intra-particle diffusion is not the only rate-limiting step governing the adsorptive process. Results from Analysis of Variance (ANOVA) confirmed that there were statistical significant differences between the adsorption efficiencies of salt activated raphia hookeri seeds (SARHS) at different time intervals (P-Value < 0.05). Tukey's Honest Significant Difference (HSD) post hoc method was employed for the identification of the location of these differences. The values calculated for ΔG°, ΔS° and ΔH° thermodynamic parameters were -29.60 KJ mol^{-1}, 0.089 KJ mol^{-1} and -0.705 KJ mol^{-1} respectively confirming that the adsorptive process is feasible, spontaneous and exothermic in nature.
© 2017 The Authors. Production and hosting by Elsevier B.V. on behalf of King Saud University. This is an open access article under the CC BY-NC-ND license (http://creativecommons.org/licenses/by-nc-nd/4.0/).

1. Introduction

Technological advances by humans have resulted in the contamination of water bodies resulting in the presence of toxic pollutants at concentrations well above the limits set by World Health Organization (WHO) and the Environmental protection agency (EPA) (Gupta et al., 2015; Celik and Demirbas, 2005; Ali and Aboul-Enein, 2006; Ali et al., 2009). The major pollution which affects the environment is water pollution (Saravanan et al., 2013a). Dyes are present in the wastewater streams of many industrial sectors such as dyeing, textile, tannery and paint industry (Bayramoglu et al., 2009). It has already been reported that the major organic compounds that constitute the increasing environmental danger are the industrial dyes and textile dyes (Saravanan et al., 2016b; Saravanan et al., 2014; Velmurugan et al., 2011). The immense development of the textile industries has contributed to the significant amount of water pollution, which is mainly due to the disposal of the industrial wastes like various inorganic and organic dyes into the water resources (Saravanan et al., 2013b,c). About 6,34,900 metric tons of dyes are produced worldwide each year and nearly 10–15% of them are discharged as effluent (Jayalakshmi et al., 2013).

Dye-containing effluents are undesirable wastewaters because they contain high level of chemicals, suspended solids, and toxic compounds (Balarak et al., 2015; Zazouli et al., 2014; Diyanati et al., 2013; Vijayakumar et al., 2012). The colour in wastewater is a consequence of inefficient processing both in the dye manufacturing and in the dye-consuming industries. The presence of this colour in very small amounts in water (less than 1 ppm for some dyes) is highly visible and undesirable from an ecological point of view as they block the penetration of the sunlight essential for photosynthesis of aquatic flora (Mittal et al., 2010). These dyes get accumulated in living tissues throughout the food chain which has human at its top (Pankaj and Harleen, 2011). Water

* Corresponding author.
E-mail address: cc.okoye@unizik.edu.ng (C.C. Okoye).
Peer review under responsibility of King Saud University.

Production and hosting by Elsevier

https://doi.org/10.1016/j.jksus.2017.11.004
1018-3647/© 2017 The Authors. Production and hosting by Elsevier B.V. on behalf of King Saud University.
This is an open access article under the CC BY-NC-ND license (http://creativecommons.org/licenses/by-nc-nd/4.0/).

Nomenclature

ANOVA	Analysis of Variance	SSE	Sum of squared errors
EB	Erythrosine B	RMS	Root mean square
PFO	Pseudo first order	Б	Intra-particle diffusion equation intercept
PSO	Pseudo second order		
RHS	*Raphia hookeri* seeds		
SARHS	Salt activated *Raphia hookeri* seed		

contamination has led the major health risks (Saravanan et al., 2016a) round the globe which is growing at a faster rate every year (Saravanan et al., 2015a,b).

Treatment of dye-containing effluents is of immense importance considering their detrimental effects when discharged untreated on the environment. Jayalakshmi et al. (2013) and Theivarasu and Mylsamy (2011) reported that industrial methods employed for treating dye wastewaters include coagulation and flocculation, photodegradation, ultrafiltration, adsorption, reverse osmosis, etc. Among them, adsorption has been found to be superior to other techniques for dye wastewater treatment in terms of cost, simplicity of design, ease of operation and insensitivity to toxic substances (Bayramoglu et al., 2009; Gupta et al., 2012; Gupta et al., 2013; Gupta and Saleh, 2013; Singh et al., 2009). Adsorption is a well-known separation process and has proved to be effective and economically feasible for the removal of various types of pollutants from effluents, especially non-biodegradable solutes (Al-Duri et al., 2005; Ali, 2010, 2012, 2014; Ali and Gupta, 2007; Ali et al., 2012).

Activated carbon adsorption systems, widely used in chemical process industries for several decades, are now playing an important role in the cleaning up of plant effluents and municipal wastewater (Norhafizah et al., 2011; Gupta et al., 1998; Ali et al., 2017, 2016a,b,c,d; Khan et al., 2011). However, commercially available activated carbon is very expensive (Velmurugan et al., 2011). The inexpensiveness of commercially produced activated carbon has encouraged the development of low-cost activated carbon from abundantly available alternatives, primarily agricultural wastes. To this effect, some researchers have reported the production of activated carbon from agricultural waste materials such as: sugar cane bagasse (Pankaj and Harleen, 2011); Meranti sawdust (Ahmad et al., 2009), coffee husks (Oliveira et al., 2008), orange peel, Neem leaves and banana peel (Velmurugan et al., 2011).

Raphia hookeri belongs to family Arecaceae (Palmae). *Raphia hookeri* is found from Gambia through the Guinea forest zone of West Africa to Cameroon, Gabon and Congo and possibly to DR Congo and Angola (Brink, 2011). Of the eight species of Raphia identified as indigenous to Nigeria, *Raphia hookeri* is the most dominant tree crop within the coastal fresh water swamp (Ndon, 2003). Raphia palm grows naturally and abundantly in the south-southern states of Nigeria. *Raphia hookeri* develops in accordance with Tomlinson's growth model. Sap tapped from the stem when the tree nears the flowering stage ferments rapidly into palm wine, a very popular drink throughout West Africa. The young terminal bud or 'palm cabbage' is eaten as a vegetable (Brink and Achigan-Dako, 2012).

Currently, there is scanty or no publication to the best of our knowledge on the usage of RHS as adsorbent for waste water treatment. In many regions of Nigeria, RHS are considered a waste product. Sequel to this and considering its abundance, we made attempts to recycle the waste material and investigate its potentiality as adsorbent. Effect of process parameters, kinetics and thermodynamics of the adsorptive process parameters were studied. In addition, ANOVA statistical tool was applied to determine if there is a practical difference between the adsorption efficiency of SARHS at different time intervals by Tukey's Honest Significant Difference test. Also the nature of the effects of treatment was also ascertained. Analysis of Variance is a statistical tool used to ascertain the differences between two or more means. Conclusions on means are done by analyzing variance therefore the nomenclature Analysis of variance is preferred to Analysis of Means. Though *t*-test could be adopted for the analysis, the advantage ANOVA has over *t*-test is that the post hoc tests of ANOVA allows better control of type 1 error.

2. Materials and methods

2.1. Materials

Raphia hookeri seeds were collected from Ugwuoba in Enugu state, Nigeria. Erythrosine B and other chemicals of analytical grades were purchased from a chemical vendor at Head Bridge, Onitsha, Anambra state, Nigeria. The reagents were used without further purification. The physical properties and molecular structure of EB are presented in Table 1.

2.2. Methods

The sample (*Raphia hookeri* seeds) collected was washed with de-ionized water to remove unwanted materials such as sand, dirt, etc., then air dried for 6 h. The sample was further oven dried at temperature of 110 °C for 4 h to ensure complete drying then size reduced to a range between 1 and 3 mm. The size reduced RHS was carbonized in a muffle furnace (SX-2.5-10) at 1173 K for 3 h, the carbonized sample was soaked in 60% by weight sodium chloride salt (NaCl) solution for 24 h at activating agent to carbonized sample ratio of 1:1 weight basis. The resulting carbon was washed with de-ionized water until the pH of the leachate was between 6 and 8, then dried in an oven at a temperature of 105 °C for 5–6 h. The activated carbon (SARHS) was cooled to room temperature in a desiccator, then size reduced to different particle sizes and stored in properly labelled air tight containers.

Stock solution (1000 mg/l) of Erythrosine B (EB) dye was prepared by dissolving 1 g of the dye in 1 L of de-ionized water. Other

Table 1
Physical properties and molecular structure of EB.

Properties	Nomenclature
Dye name	Erythrosine B
Dye Colour	Cherry pink
Chemical formula	$C_{20}H_6I_4Na_2O_5$
IUPAC name	2-(6-Hydroxy-2,4,5,7-tetraiodo-3-oxo-xanthen-9-yl) benzoic acid
Molecular weight	879.86 g/mol
λ_{max}	530 nm
Molecular structure	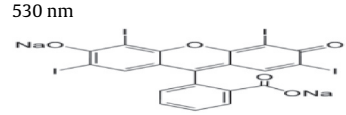

concentrations of the dye were prepared by serial dilution of the stock solution.

2.3. Physicochemical characterization of SARHS

The methodology for the physicochemical characterization of the activated carbon produced is reported in our earlier published journal (Okoye et al., 2016).

2.3.1. Instrumental characterization

The instrumental characterization of the sample was determined using the scanning electron microscope (model Phonem Prox) and the FTIR spectrophotometer (Shimadzu FTIR 8400). Result from FTIR spectra was used to identify the functional groups present in the activated carbon. The morphology of the activated carbon was displayed by SEM micrograph.

2.4. Adsorption tests

Sorption experiments were conducted to evaluate the adsorptive performance of SARHS at different temperatures (30–60 °C). The experiments were performed at optimum results of 75 μm adsorbent particle size, 1 g adsorbent dosage, 100 mg/L adsorbate concentration, and pH 4 obtained in preliminary experiments. The steps for the sorption experiment are described below:

1. A number of different 250 ml Pyrex beakers containing 100 ml of 100 mg/L concentration of EB dye and specified dosage of SARHS were set at 30 °C, 40 °C, 50 °C, 60 °C respectively.
2. The beakers containing the mixtures were stirred using a magnetic stirrer at speed of 110 rev/min for 150 min.
3. At the elapse of the set time for the treatment, the mixture was filtered using Whatman No. 1 filter paper.
4. The amount of unadsorbed dye in each supernatant solution was tested using a Visible spectrophotometer.

The percentage of dye adsorbed and sorption capacity (mg/g) were calculated from Eqs. (1) and (2):

$$\%Adsorbed = \frac{C_o - C_e}{C_o} \times 100 \tag{1}$$

$$q_e = \frac{(C_o - C_e)V}{m} \tag{2}$$

where q_e is the amount of dye adsorbed (mg/g), m is the weight of adsorbent (g), V, volume of the dye solution and C_o and C_e, the dye concentration (mg/L) at the initial time and at a time t, respectively.

2.5. Adsorption kinetics

Solute uptake rate is evaluated by adsorptive kinetics study. Various models have been proposed to describe and clarify pollutant adsorption mechanism (Annadurai et al., 2008). As a rule, models based on the apparent reaction order of adsorption (pseudo-first order and pseudo-second order models) are used to describe the kinetics of the sorption of dyes onto sorbents (Janoš et al., 2007). However, because the aforementioned kinetics models cannot give definite mechanism, another simplified model (Intra-particle diffusion kinetic model) is also tested (Kushwaha et al., 2008). Therefore, the experimental data were fitted into non-linearized PFO and PSO; linearized Intra-particle diffusion kinetic model equations.

2.5.1. Pseudo-first order

Lagergren proposed that the rate of adsorption of solute on the adsorbent is based on the adsorption capacity and followed a pseudo-first order equation. The pseudo-first order kinetic model equations can be expressed as follows (Bellir et al., 2010):

$$\frac{dq_t}{dt} = k_1(q_e - q_t) \tag{3}$$

where k_1 is the rate constant of the model, q_t is the amount of solute adsorbed on the adsorbent at time t, and q_e is the amount at equilibrium. Integrating and applying boundary conditions $q_t = 0$ at $t = 0$ and $q_t = q_t$ at $t = t$, the natural logarithmic form of Eq. (3) was obtained:

$$\ln(q_e - q_t) = \ln q_e - k_1 t \tag{4}$$

Rearranging Eq. (4), the non linear form of the pseudo-first order kinetic equation is stated as:

$$q_t = q_e(1 - e^{-k_1 t}) \tag{5}$$

2.5.2. Pseudo-second order

The non-linear pseudo-second order kinetic model equation is expressed as:

$$q_t = \frac{k_2 q_e^2 t}{1 + k_2 q_e t} \tag{6}$$

where k_2 is pseudo-second order rate constant.

2.5.3. Intra-particle diffusion model

The fractional uptake of the solute on particle, F, in a liquid-solid system will vary with the function (Allen et al., 1989):

$$\frac{D_0 t^{0.5}}{r^2} \tag{10}$$

Hence there is a linear relationship between F and $t^{0.5}$ for much of the adsorption process. F can be defined as:

$$F = \frac{(C_0 - C_t)}{C_0} \tag{11}$$

The Intra-particle diffusion parameter, k_i, can be defined as the linear gradient of a graph of the amount of dye adsorbed per gram of adsorbent (q_t) against the square root of time, $t^{0.5}$. Hence the diffusion rate parameter, k_i, is evaluated from:

$$k_i = \frac{1}{t^{0.5}} q_t \tag{12}$$

Rearranging Eq. (12),

$$q_t = k_i t^{0.5} \tag{13}$$

2.6. Kinetic models validity

The best fit between PFO and PSO kinetic models was determined by the sum of squared errors (SSE%), root mean square (RMS) and coefficient of determination (R^2):

$$SSE(\%) = \frac{\sum (q_{e,exp} - q_{t,cal})^2}{N} \tag{7}$$

$$RMS = \sqrt{\frac{1}{N}\sum_{i=1}^{N}\left(\frac{q_{e,exp} - q_{t,cal}}{q_{eexp}}\right)^2} \tag{8}$$

$$R^2 = \frac{\sum (q_{t,cal} - \bar{q}_{t,exp})^2}{\sum (q_{t,cal} - \bar{q}_{t,exp})^2 + \sum (q_{t,cal} - q_{t,exp})^2} \tag{9}$$

where N and $q_{e,exp}$ are the number of data points and amount of the dye adsorbed at equilibrium per unit mass of adsorbent respectively. $q_{t,exp}$ and q_{tcal} are experimental and calculated adsorption amount of the dye adsorbed at time t, respectively. The average of

$q_{t,exp}$ is represented by $\bar{q}_{t,exp}$. The lower the value of SSE, the better the goodness of fit (Ramachandran et al., 2011). The higher the value of R^2 and the lower the value of the RMS, the better will be the goodness of fit (Kitanovic et al., 2008).

2.7. Statistical comparative analysis

2.7.1. Analysis of variance

Analysis of Variance is an effective statistical tool for comparing the means of two or more independent groups.

2.7.2. Tukey's honest significant difference (HSD) test

Tukey's test calculates a new critical value that can be used to evaluate if differences between any two pairs of means are significant. The critical value is a little different because it involves the mean difference that has to be exceeded to achieve significance. So one simply calculates one critical value and then the difference between all possible pairs of means. Each difference is then compared to the Tukey critical value. If the difference is larger than the Tukey value, the comparison is significant (Newsom, 2013).

2.8. Adsorption thermodynamics

Thermodynamic parameters (standard free energy (ΔG°), standard enthalpy change (ΔH°) and standard entropy change (ΔS°) were evaluated from the following equations (Bayramoglu et al., 2009):

$$\Delta G^{\circ} = -RT\ 1n\ K_a \tag{14}$$

The Gibb's free energy, enthalpy change and entropy change at constant temperature are related by the following equations:

$$\Delta G^{\circ} = \Delta H^{\circ} - T\Delta S^{\circ} \tag{15}$$

$$\ln K_a = \left(\frac{\Delta S^{\circ}}{R}\right) - \left(\frac{\Delta H^{\circ}}{RT}\right) \tag{16}$$

where K_a is the dependency of the equilibrium association constant (K_a = b, from Langmuir constant, L/mol), R is the universal gas constant (8.314 J mol^{-1} K^{-1}). It is well known that the unit for ΔG is J mol^{-1}. Since the unit for the term RT is also J mol^{-1}, the equilibrium constant K in Eq. (14) must be dimensionless. If adsorption was

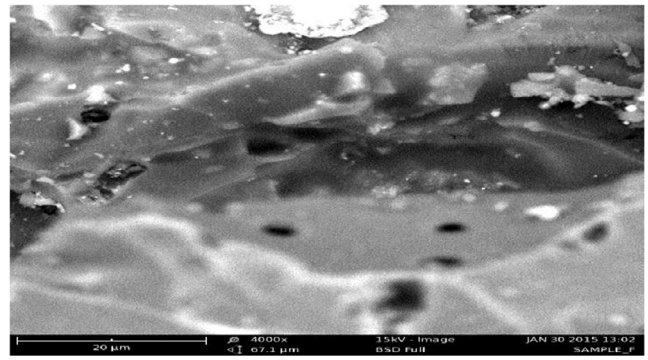

Fig. 2. SEM micrograph of SARHS.

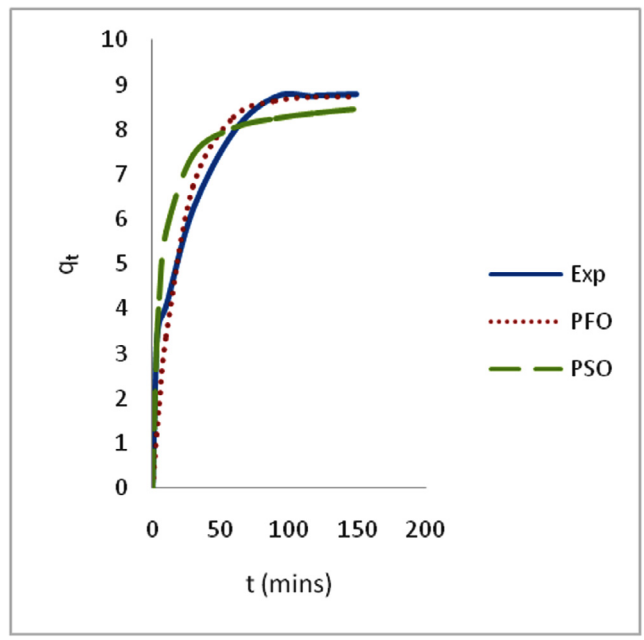

Fig. 3. Non linear plots of measured and modeled time profiles for the adsorption of EB dye on SARHS at 30 °C.

Table 2
Physical properties of SARHS.

Sample	Surface area (m^2/g)	Ash content (%)	Moisture content (%)	pH	Bulk density (g/cm^{-2})
AAAE	181	6.01	8.5	7.4	0.72

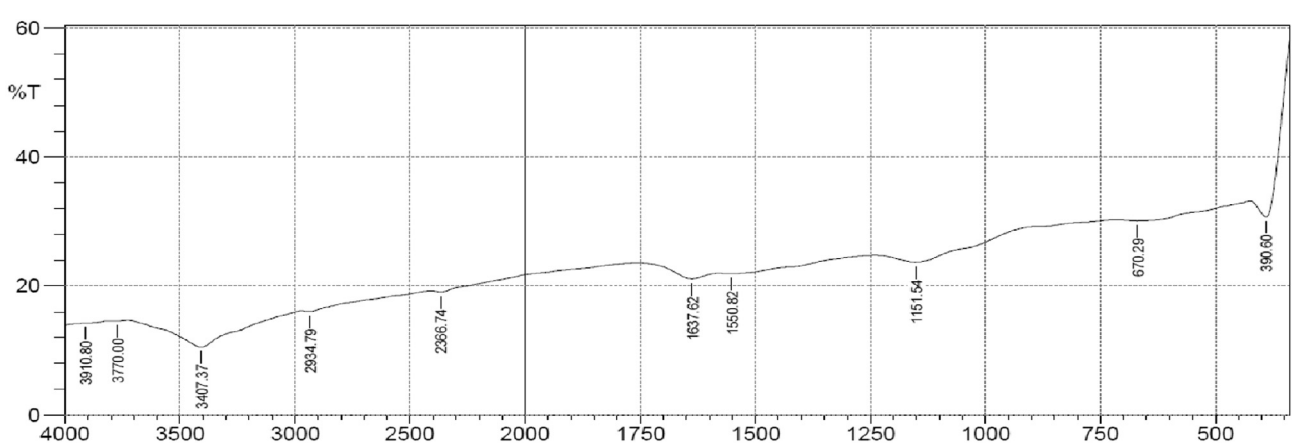

Fig. 1. FTIR Spectrum of SARHS.

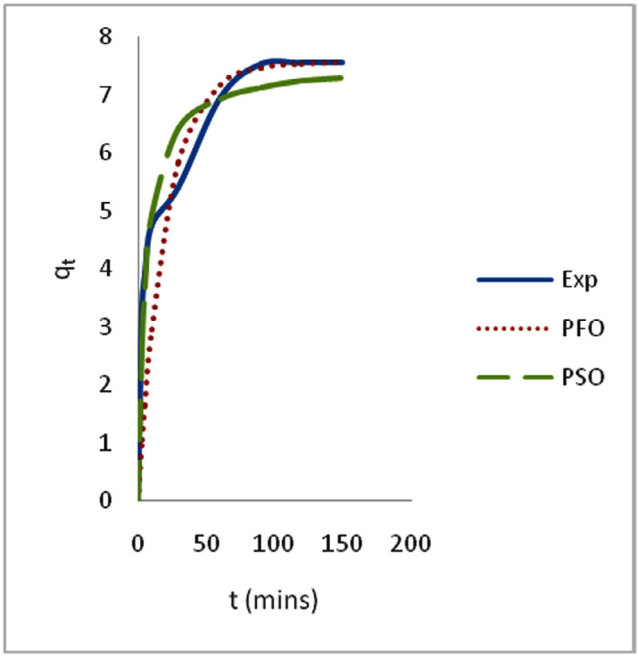

Fig. 4. Non linear plots of measured and modeled time profiles for the adsorption of EB dye on SARHS at 40 °C.

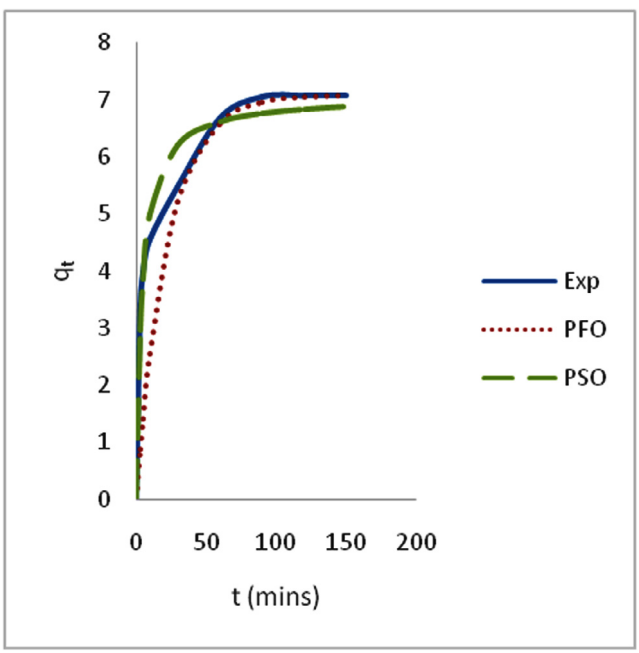

Fig. 5. Non linear plots of measured and modeled time profiles for the adsorption of EB dye on SARHS at 50 °C.

investigated from an aqueous solution and if K is given in L/mol, then K can be easily recalculated as dimensionless by multiplying it by 55.5 (number of moles of water per liter of solution) (Milonjić, 2007), T is the solution temperature.

3. Results and discussion

3.1. Properties of SARHS

Characterization results for the activated carbon (SARHS) were presented in Table 2. The following physical properties were investigated: surface area, ash content, moisture content, pH and bulk density. From Table 2, the high value of surface area obtained shows that SARHS is highly porous while the low value of ash content shows that the produced activated carbon has low inorganic content and high fixed carbon. Any porous material will have the tendency to adsorb moisture. The moisture content of SARHS is comparable with the values also reported by Sivakumar et al. (2012). The pH value reported in Table 2 is in the range of 6.8–7.4. It has been reported by Ekpete and Horsfall (2011) that for most applications, carbon pH 6–8 is acceptable.

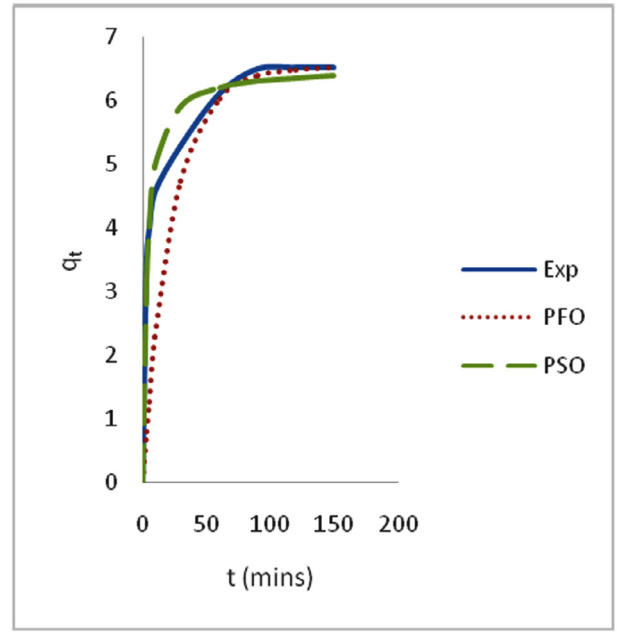

Fig. 6. Non linear plots of measured and modeled time profiles for the adsorption of EB dye on SARHS at 60 °C.

3.2. Instrumental characteristics of SARHS

Fig. 1 is a graph of %Transmittance vs wave number for SARHS. The FTIR spectrum identified the functional groups on the activated carbon surface. Peaks 3910.80 cm^{-1} and 3770.00 cm^{-1} show the presence of O–H stretch in phenol and alcohols, 3407.37 cm^{-1} was assigned to O–H stretch, H-bonded, alcohols, phenols, 2934.79 cm^{-1} (C–H stretching) shows the presence of aliphatic hydrocarbon groups. Peaks 2366.74 cm^{-1}, 1637.62 cm^{-1} and 1550.82 depict the presence of C≡C bonds, C=O bonds, and C=C stretching respectively. Other bands detected can be assigned to in-plane C—H bending (1151.54 cm^{-1}) and =C—H out of plane bending (670.29 cm^{-1}).

3.2.1. SEM analysis

The surface morphology of SARHS was investigated by the scanning electron micrograph. Fig. 2 shows a relatively fibrous surface with sponge-like protrusions, pores and cavities of different sizes. The characteristics observed on the external structure of the adsorbent (SARHS) may be as a result of removal of some volatile matters during carbonization and also, evaporation of the impregnating materials which occupied some space on the carbon structure.

3.3. Kinetics parameters

Adsorption is time-dependent process and it is very important to know the rate of adsorption for design and evaluation of the

Table 3
Kinetic data for adsorption of EB on SARHS.

Temp	PFO				PSO				Intra-particle diffusion		
	K_1	R^2	RMS	SSE	K_2	R^2	RMS	SSE	K_i	Б	R^2
30	0.0488	0.9012	0.291	1.023	0.0215	0.8621	0.169	0.785	0.9120	4.228	0.7947
40	0.0497	0.8081	0.347	1.330	0.0250	0.9229	0.103	0.485	0.5997	4.536	0.8244
50	0.0444	0.7694	0.382	1.465	0.0337	0.9339	0.080	0.381	0.5086	4.540	0.7969
60	0.0431	0.7172	0.408	1.602	0.0490	0.9341	0.064	0.306	0.3951	4.542	0.8213

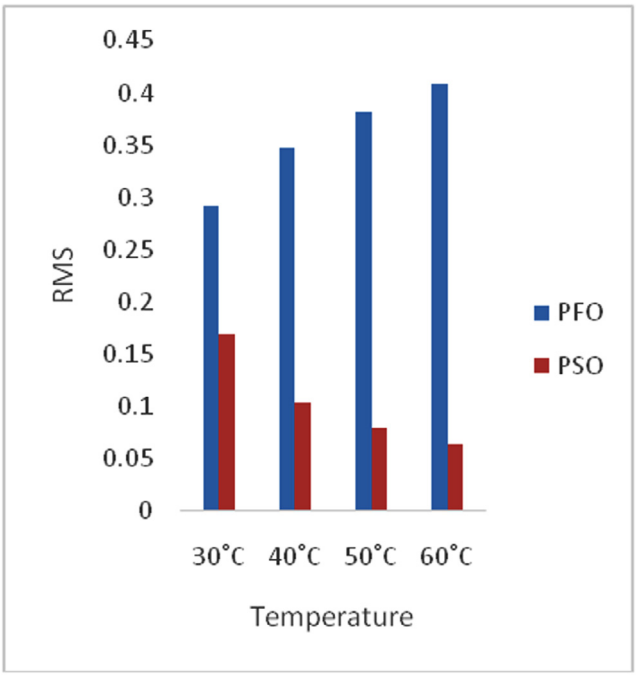

Fig. 7. Comparative variation of RMS with temperature for PFO and PSO.

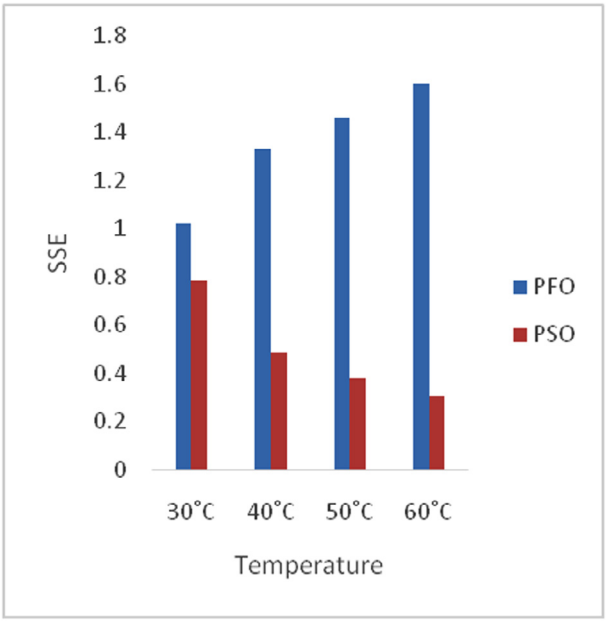

Fig. 8. Comparative variation of SSE with temperature for PFO and PSO.

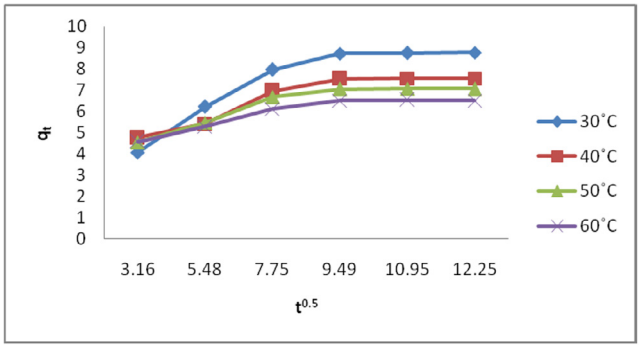

Fig. 9. Linearized Intra-particle diffusion plot for the adsorption of EB dye on SARHS.

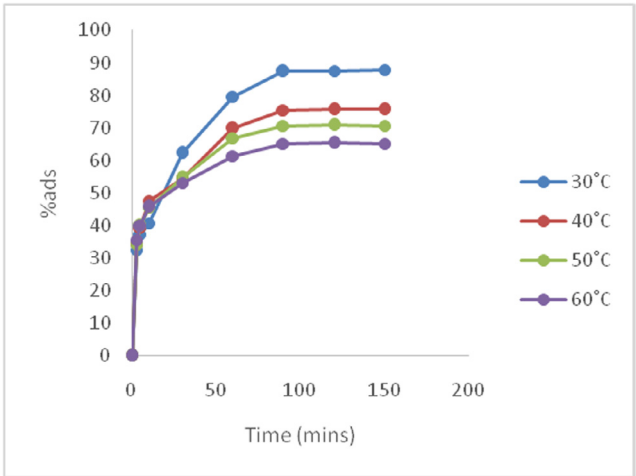

Fig. 10. Time lined adsorptive efficiency variation at different temperatures.

adsorbent in removing the dyes in wastewater (Zawani et al., 2009). In order to examine the controlling mechanism of biosorption process such as mass transfer and chemical reaction, kinetics models were used to test the experimental data (Bayramoglu et al., 2009). The kinetics study for the adsorption of EB on SARHS was investigated using the PFO and PSO kinetic models. Figs. 3–6 show non-linear plots of the models under investigation. The parameters of the kinetic models k_1 and k_2 presented in Table 3 were estimated from the experimental data by applying the golden search method. It is observed from Figs. 3–6 that the system's equilibration time is 90 min. The rate of the dye adsorbed diminished after 90 min possibly due to the fact that at start-up of the experiments, all the reaction sites were vacant and hence the extent of removal was high but decreases over time. The values calculated for RMS (Eq. (7)), SSE (Eq. (8)) and coefficient of determination, R^2 (Eq. (9)) presented in Table 3 were used for quantitative comparison of the applicability of the models investigated. The

Table 4
ANOVA table for effect of time variation on the adsorptive performance of SARHS.

	Sum of Squares	Df	Mean Square	F	Sig.
Between Groups	8318.077	7	1188.297	26.432	.000
Within Groups	1078.955	24	44.956		
Total	9397.031	31			

Table 5
Tukey's HSD post hoc tests analysis for the effect of varying time on performance.

(I) Time	(J) Time	Mean Difference (I-J)	Std. Error	Sig.	95% Confidence Interval	
					Lower Bound	Upper Bound
3.00	5.00	−5.05000	4.74112	.958	−20.7522	10.6522
	10.00	−10.85750	4.74112	.339	−26.5597	4.8447
	30.00	−22.01000*	4.74112	.002	−37.7122	−6.3078
	60.00	−35.33750*	4.74112	.000	−51.0397	−19.6353
	90.00	−40.62750*	4.74112	.000	−56.3297	−24.9253
	120.00	−40.79750*	4.74112	.000	−56.4997	−25.0953
	150.00	−40.79500*	4.74112	.000	−56.4972	−25.0928
5.00	3.00	5.05000	4.74112	.958	−10.6522	20.7522
	10.00	−5.80750	4.74112	.916	−21.5097	9.8947
	30.00	−16.96000*	4.74112	.028	−32.6622	−1.2578
	60.00	−30.28750*	4.74112	.000	−45.9897	−14.5853
	90.00	−35.57750*	4.74112	.000	−51.2797	−19.8753
	120.00	−35.74750*	4.74112	.000	−51.4497	−20.0453
	150.00	−35.74500*	4.74112	.000	−51.4472	−20.0428
10.00	3.00	10.85750	4.74112	.339	−4.8447	26.5597
	5.00	5.80750	4.74112	.916	−9.8947	21.5097
	30.00	−11.15250	4.74112	.308	−26.8547	4.5497
	60.00	−24.48000*	4.74112	.001	−40.1822	−8.7778
	90.00	−29.77000*	4.74112	.000	−45.4722	−14.0678
	120.00	−29.94000*	4.74112	.000	−45.6422	−14.2378
	150.00	−29.93750*	4.74112	.000	−45.6397	−14.2353
30.00	3.00	22.01000*	4.74112	.002	6.3078	37.7122
	5.00	16.96000*	4.74112	.028	1.2578	32.6622
	10.00	11.15250	4.74112	.308	−4.5497	26.8547
	60.00	−13.32750	4.74112	.139	−29.0297	2.3747
	90.00	−18.61750*	4.74112	.012	−34.3197	−2.9153
	120.00	−18.78750*	4.74112	.011	−34.4897	−3.0853
	150.00	−18.78500*	4.74112	.011	−34.4872	−3.0828
60.00	3.00	35.33750*	4.74112	.000	19.6353	51.0397
	5.00	30.28750*	4.74112	.000	14.5853	45.9897
	10.00	24.48000*	4.74112	.001	8.7778	40.1822
	30.00	13.32750	4.74112	.139	−2.3747	29.0297
	90.00	−5.29000	4.74112	.947	−20.9922	10.4122
	120.00	−5.46000	4.74112	.938	−21.1622	10.2422
	150.00	−5.45750	4.74112	.938	−21.1597	10.2447
90.00	3.00	40.62750*	4.74112	.000	24.9253	56.3297
	5.00	35.57750*	4.74112	.000	19.8753	51.2797
	10.00	29.77000*	4.74112	.000	14.0678	45.4722
	30.00	18.61750*	4.74112	.012	2.9153	34.3197
	60.00	5.29000	4.74112	.947	−10.4122	20.9922
	120.00	−.17000	4.74112	1.000	−15.8722	15.5322
	150.00	−.16750	4.74112	1.000	−15.8697	15.5347
120.00	3.00	40.79750*	4.74112	.000	25.0953	56.4997
	5.00	35.74750*	4.74112	.000	20.0453	51.4497
	10.00	29.94000*	4.74112	.000	14.2378	45.6422
	30.00	18.78750*	4.74112	.011	3.0853	34.4897
	60.00	5.46000	4.74112	.938	−10.2422	21.1622
	90.00	.17000	4.74112	1.000	−15.5322	15.8722
	150.00	.00250	4.74112	1.000	−15.6997	15.7047
150.00	3.00	40.79500*	4.74112	.000	25.0928	56.4972
	5.00	35.74500*	4.74112	.000	20.0428	51.4472
	10.00	29.93750*	4.74112	.000	14.2353	45.6397
	30.00	18.78500*	4.74112	.011	3.0828	34.4872
	60.00	5.45750	4.74112	.938	−10.2447	21.1597
	90.00	.16750	4.74112	1.000	−15.5347	15.8697
	120.00	−.00250	4.74112	1.000	−15.7047	15.6997

* The mean difference is significant at the 0.05 level.

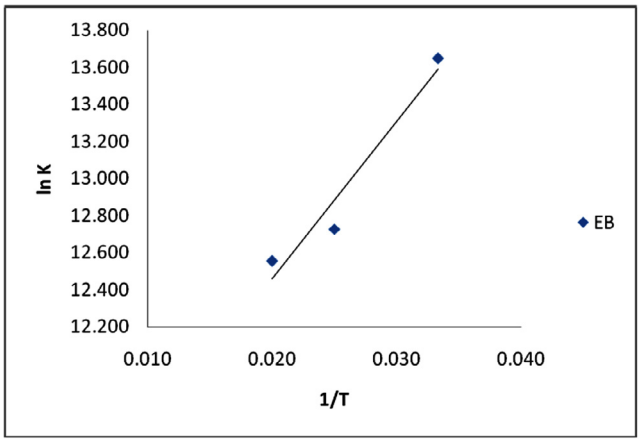

Fig. 11. Thermodynamic plot of lnK vs 1/T for adsorption of EB on SARHS.

Table 6
Thermodynamic parameters for the adsorption of EB on SARHS.

Adsorbent	Thermodynamics Parameters			
	T(K)	ΔG° (kJ/mol)	ΔH° (kJ/mol)	ΔS° (kJ/mol.K)
SARHS	303	−27.814		
	313	−28.709	−0.705	0.089
	323	−29.603		

histogram plots (Figs. 7 and 8) depicted that irrespective of the temperature under study, PSO had lower values for RMS and SSE. From Table 3, it is also seen that PSO generally has calculated coefficient of determination values (R^2) closer to unity hence, PSO better fitted the experimental data obtained for the adsorption of EB dye on SARHS.

Fig. 9 is a plot of linearized intra-particle diffusion model equation. At varying temperatures under consideration, it is observed that the plots generally follow the same trend and did not pass through the origin. The deviation observed from the point of origin may be as a result of rate of mass transfer difference at the initial and final periods of the adsorptive process. The deviation of the plots from the origin is an indication that intra-particle diffusion does not solely determine the rate-limiting step, possibly both intra-particle diffusion and surface adsorption contribute to the rate determining step. The non-passage of the plots through the origin may also be as a result of some degree of boundary layer control. According to Bayramoglu et al. (2009), the intercept (Б) of the plot of q_t versus time$^{0.5}$ gives an idea about boundary layer thickness, the larger the value of the intercept, the greater the boundary layer diffusion effect is. The two linear portions of the Intra-particle diffusion plot show that the first linear portion of the plot indicates the boundary layer effect on the adsorption and the second linear portion of the plot indicates the intra-particle diffusion (Senthil et al., 2012).

3.4. Statistical analyses

3.4.1. One-way factorial analyses for the effect of temperature variation

Fig. 10 shows the effect of temperature on the time-based adsorptive performance of EB dye on SARHS. It was recorded that the highest percentage of dye adsorbed at temperatures 30 °C, 40 °C, 50 °C and 60 °C are 87.78%, 75.56%, 70.7% and 65.21% respectively thus there is an inverse proportional relationship between temperature and percentage of EB dye adsorbed on SARHS.

Analysis of Variance (ANOVA) was used to ascertain if there was a practical difference between the adsorption efficiency of SARHS at different time intervals. This investigation was carried out to establish that the different adsorptive performance at various time intervals was not by chance. The probability value recorded in Table 4 was lower than the critical value (0.05) thus the null hypothesis was rejected and as such the alternate hypothesis was accepted (there were statistical significant differences at various time intervals among the adsorptive performances of EB dye on SARHS).

A significant F-value recorded in Table 4 also reveals that there are differences in the means but did not disclose where the differences are. To identify the location of these differences, Tukey's HSD post hoc method of analysis was adopted.

Table 5 shows Tukey's HSD post hoc analysis for the effect of varying time on the adsorptive performance of EB on SARHS. P-values for these groups: 3 and 30 min, 60 min, 90 min, 120 min and 150 min, 5 and 30 min, 60 min, 90 min, 120 min and 150 min, 10 and 60 min, 90 min, 120 min and 150 min, 30 and 3 min, 5 min, 90 min, 120 min and 150 min, 60 and 3 min, 5 min and 10 min, 90 and 3 min, 5 min, 10 min and 30 min, 120 and 3 min, 5 min, 10 min and 30 min, 150 and 3 min, 5 min, 10 min and 30 min are less than 0.05 therefore, depict statistical significant difference in their adsorptive performances. Table 5 shows that there is no significant difference (between these compared times: 3 and 5 min, 10 min; 5 and 3 min, 10 min; 10 and 3 min, 5 min; 30 and 10 min, 60 min; 90 and 60 min, 120 min, 150 min; 120 and 60 min, 90 min, 150 min; 150 and 60 min, 90 min, 120 min. However, the P-values for these timings: 3 and 5 min, 5 and 10 min, 60 and 90 min, 120 min and 150 min are very close to unity therefore showing very high level of no statistical significance between the compared time intervals. The equilibrium time for the adsorption of EB on SARHS was established around 90 min. This finding is in line with the observation on Figs. 3 and 4.

3.5. Adsorption thermodynamics

Thermodynamic parameters were estimated from van't Hoff's plot (Fig. 11). From the slope and intercept of the graph, the values of ΔH° and ΔS° were calculated. The values for change in Gibbs free energy (ΔG°) were calculated from Eq. (15). The calculated values were presented in Table 6. The negative values of ΔG° at all temperature under investigation depict that the process is feasible and spontaneous in nature. A negative value of ΔH° indicates that the adsorption process is exothermic. The positive change in entropy value obtained is an indication of an increased randomness between solid-solution interfaces during the adsorption of EB dye on SARHS (Hossain et al., 2012; Rameshraja et al., 2012).

4. Conclusion

RHS, a novel precursor, was shown to have strong potential for use as an adsorbent for the treatment of dye based wastewater. The percentage uptake of EB dye on SARHS is temperature dependent. An equilibration time of 90 minutes is sufficient for 87.78% adsorption of EB on SARHS at the experimental condition of 1 g dosage, 30 °C and 100 mg/L adsorbate concentration. The experimental data better fitted the PSO kinetic model. ANOVA calculations reveal that there were statistical significant differences between the adsorption efficiency of SARHS at different time intervals. It can be concluded from the results obtained that the low cost and eco-friendly material (SARHS) can be used as an available alternative adsorbent for dye removal in wastewater treatment.

References

Ahmad, A., Rafatullah, M., Sulaiman, O., Ibrahim, M.H., Hashim, R., 2009. Scavenging behaviour of meranti sawdust in the removal of methylene blue from aqueous solution. J. Hazard. Mater. 170, 357–365.

Al-Duri, B., Magdy, Y., Saad, R., McKay, G., 2005. Modelling of multicomponent equilibrium for the adsorption of basic dyes onto bagasse pith. Inst. Chem. Eng. 69, 246–254.

Ali, I., 2010. The quest for active carbon adsorbent substitutes: Inexpensive adsorbents for toxic metal ions removal from wastewater. Sep. Purif. Rev. 39, 95–171.

Ali, I., 2012. New generation adsorbents for water treatment. Chem. Rev. 112 (10), 5073–5091.

Ali, I., 2014. Water treatment by adsorption columns: evaluation at ground level. Sep. Purif. Rev. 43 (3), 175–205.

Ali, I., Aboul-Enein, H.Y., 2006. Instrumental Methods in Metal Ions Speciation: Chromatography, Capillary Electrophoresis and Electrochemistry. Taylor & Francis Ltd, New York. ISBN: 0-8493-3736-4.

Ali, I., Aboul-Enein, H.Y., Gupta, V.K., 2009. Nano Chromatography and Capillary Electrophoresis: Pharmaceutical and Environmental Analyses. Wiley & Sons, Hoboken, USA. ISBN: 978-0-470-17851-5.

Ali, I., Asim, M., Khan, T.A., 2012. Low cost adsorbents for removal of organic pollutants from wastewater. J. Environ. Manage. 113, 170–183.

Ali, I., Gupta, V.K., 2007. Advances in water treatment by adsorption technology. Nat. Protocol 1, 2661–2667.

Ali, I., Al-Othman, Z.A., Alwarthan, A., 2016a. Green synthesis of functionalized iron nano particles and molecular liquid phase adsorption of ametryn from water. J. Mol. Liq. 221, 1168–1174.

Ali, I., Al-Othman, Z.A., Alwarthan, A., 2016b. Synthesis of composite iron nano adsorbent and removal of ibuprofen drug residue from water. J. Mol. Liq. 219, 858–864.

Ali, I., Al-Othman, Z.A., Alwarthan, A., 2016c. Molecular uptake of congo red dye from water on iron composite nano particles. J. Mol. Liq. 224, 171–176.

Ali, I., Al-Othman, Z.A., Alharbi, O.M.L., 2016d. Uptake of pantoprazole drug residue from water using novel synthesized composite iron nano adsorbent. J. Mol. Liq. 218, 465–472.

Ali, I., Alothman, Z.A., Alwarthan, A., 2017. Uptake of propranolol on ionic liquid iron nanocomposite adsorbent: kinetic, thermodynamics and mechanism of adsorption. J. Mol. Liq. 236, 205–213.

Allen, S.J., McKay, G., Khader, K.Y.H., 1989. Intraparticle diffusion of a basic dye during adsorption onto sphagnum peat. Environ. Pollut. 56, 39–50.

Annadurai, G., Ling, L.Y., Lee, J.F., 2008. Adsorption of reactive dye from an aqueous solution by chitosan: isotherm, kinetic and thermodynamic analysis. J. Hazard. Mater. 152 (1), 337–346.

Balarak, D., Jaafari, J., Hassani, G., Mahdavi, Y., Tyagi, I., Agarwal, S., Gupta, V.K., 2015. The use of low-cost adsorbent (Canola residues) for the adsorption of methylene blue from aqueous solution: isotherm, kinetic and thermodynamic studies. Colloids Interface Sci. Commun. 7, 16–19.

Bayramoglu, G., Altintas, B., Arica, M., 2009. Adsorption kinetics and thermodynamic parameters of cationic dyes from aqueous solutions by using a new strong cation- exchange resin. Chem. Eng. J. 152, 339–346.

Bellir, K., Bencheikh, M., Meniai, A., 2010. Removal of methylene blue from aqueous solutions using acid activated Algerian bentonite: equilibrium and kinetic study. International Renewable Energy Congress, Tunisia. Nov 5–7.

Brink, M. (2011). Raphia hookeri PROTA (Plant Resources of Tropical Africa/ Resources, Wageningen, Netherlands. Retrieved from http://www.prota4u.org/search.asp, 20/12/13.

Brink, M., Achigan-Dako, E.G., 2012. Plant Resources of Tropical Africa. PROTA Foundation, Wageningen.

Celik, A., Demirbas, A., 2005. Removal of heavy metal ions from aqueous solutions via adsorption onto modified lignin from pulping wastes. Energy Source 27, 1167–1177.

Diyanati, R.A., Balarak, D., Ghasemi, M., 2013. Survey of efficiency agricultural waste in removal of acid orange 7 (AO7) dyes from aqueous solution: kinetic and equilibrium study. Iran. J. Health Sci. 2, 35–40.

Ekpete, O.A., Horsfall, M.J., 2011. Preparation and characterization of activated carbon derived from fluted pumpkin stem waste *(Telfairia occidentalis Hook F)*. Res. J. Chem. Sci. 1 (3).

Gupta, V.K., Srivastava, S.K., Mohan, D., Sharma, S., 1998. Design parameters for fixed bed reactors of activated carbon developed from fertilizer waste for the removal of some heavy metal ions. Waste Manage. (Oxford) 17 (8), 517–522.

Gupta, V.K., Mittal, A., Jharec, D., Mittalc, J., 2012. Batch and bulk removal of hazardous colouring agent Rose Bengal by adsorption techniques using bottom ash as adsorbent. RSC Adv. 2, 8381–8389.

Gupta, V.K., Rajeev, K., Arunima, N., Saleh, T.A., Barakart, M.A., 2013. Adsorptive removal of dyes from aqueous solution onto carbon nanotubes: a review. Adv. Colloid Interface Sci. https://doi.org/10.1016/j.cis.2013.03.003.

Gupta, V.K., Nayak, A., Agarwal, S., 2015. Bioadsorbents for remediation of heavy metals: current status and their future prospects. Environ. Eng. Res. 20 (1), 1–18.

Gupta, V.K., Saleh, T.A., 2013. Sorption of pollutants by porous carbon, carbon nanotubes and fullerene - an overview. Environ. Sci. Pollut. Res. https://doi.org/10.1007/s11356-013-1524-1.

Hossain, M.A., Ngo, H.H., Guo, W.S., Setiadi, T., 2012. Adsorption and desorption of copper(II)ions onto garden grass. Bioresour. Technol. 121, 386–395.

Janoš, P., Michálek, P., Turek, L., 2007. Sorption of ionic dyes onto unsaturated low-rank coal-oxihumolite: a kinetic study. Dyes Pigm. 74, 363.

Jayalakshmi, L., Devadoss, V., Ananthakumar, K., 2013. Adsorption of acid orange-7 dye onto activated carbon produced from bentonite - a study of equilibrium adsorption isotherm. Chem. Sci. Trans. 2 (S1), S7–S12.

Khan, T.A., Sharma, S., Ali, I., 2011. Adsorption of Rhodamine B dye from aqueous solution onto acid activated mango (Magnifera indica) leaf powder: equilibrium, kinetic and thermodynamic studies. J. Toxicol. Environ. Health Sci. 3 (10), 286–297.

Kitanovic, S., Milenovic, D., Veeljkovic, V.B., 2008. Empirical kinetic models for the resinoid extraction from aerial parts of St John's Wort (Hypericum perforatum L.). J. Biochem. Eng 41, 1–11.

Kushwaha, S., Sodaye, S., Padmaja, P., 2008. Equilibrium, kinetics and thermodynamic studies for adsorption of Hg(II) on palm shell powder. World Acad. Sci. Technol. 43, 600–606.

Milonjić, S.K., 2007. A consideration of the correct calculation of thermodynamic parameters of adsorption. J. Serb. Chem. Soc. 72 (12), 1363–1367.

Mittal, A., Mittal, J., Malviya, A., Kaur, D., Gupta, V.K., 2010. Decoloration treatment of a hazardous triarylmethane dye, Light Green SF (Yellowish) by waste material adsorbents. J. Colloid Interface Sci. 342, 518–527.

Ndon, D.S., 2003. The Raphia Palm. Concept Publications Ltd, Lagos.

Newsom, 2013. In: Post Hoc Tests. Spring: USP 634 Data Analysis I, pp. 1–13.

Norhafizah, B.A.H., Nurul, A.B.R., Wong, C.S., 2011. Removal of Cu(II) from water by adsorption on papaya seed. Asian Trans. Eng. 1 (5), 49–55.

Okoye, C.C., Onukwuli, O.D., Okey-Onyesolu, C.F., Nwokedi, I.C., 2016. Adsorptive removal of Erythrosin B dye onto *Terminalia Catappa* endocarp prepared activated carbon: kinetics, isotherm and thermodynamics studies. Chem. Process Eng. Res. 43, 26–43.

Oliveira, L.S., Franca, A.S., Alves, T.M., Rocha, S.D.F., 2008. Evaluation of untreated coffee husks as potential biosorbents for treatment of dye contaminated waters. J. Hazard. Mater. 155, 507–512.

Pankaj, S., Harleen, K., 2011. Sugarcane bagasse for the removal of erythrosine B and methylene blue from aqueous waste. Appl. Water Sci. 1, 135–145.

Ramachandran, P., Vairamuthu, R., Ponnusamy, S., 2011. Adsorption isotherms, kinetics, thermodynamics and desorption studies of reactive orange 16 on activated carbon derived from *Ananas cosmosus* (L.) carbon. ARPN J. Eng. Appl. Sci. 6 (11), 15–26.

Rameshraja, D., Srivastava, V.C., Kushwaha, J.P., Mall, I.D., 2012. Quinoline adsorption onto granular activated carbon and bagasse fly ash. Chem. Eng. J. 181–182, 343–351.

Saravanan, R., Thirumal, E., Gupta, V.K., Narayanan, V., Stephen, A., 2013a. The photocatalytic activity of ZnO prepared by simple thermal decomposition method at various temperatures. J. Mol. Liq. 177 (2013), 394–401.

Saravanan, R., Karthikeyan, S., Gupta, V.K., Sekaran, G., Narayanan, V., Stephen, A., 2013b. Enhanced photocatalytic activity of ZnO/CuO nanocomposite for the degradation of textile dye on visible light illumination. Mater. Sci. Eng., C 33, 91–98.

Saravanan, R., Karthikeyan, N., Gupta, V.K., Thirumal, E., Thangadurai, P., Narayanan, V., Stephen, A., 2013c. ZnO/Ag nanocomposite: an efficient catalyst for degradation studies of textile effluents under visible light. Mater. Sci. Eng., C 33, 2235–2244.

Saravanan, R., Gupta, V.K., Narayanan, V., Stephen, A., 2014. Visible light degradation of textile effluent using novel catalyst ZnO/g-Mn2O3. J. Taiwan Inst. Chem. Eng. 45, 1910–1917.

Saravanan, R., Khan, M. Mansoob, Gupta, V.K., Mosquera, E., Gracia, F., Narayanang, V., Stephen, A., 2015a. ZnO/Ag/Mn2O3 nanocomposite for visible light induced industrial textile effluent degradation, uric acid and ascorbic acid sensing and antimicrobial activity. RSC Adv. 2015 (5), 34645–34651.

Saravanan, R., Mansoob Khan, M., Gupta, V.K., Mosquera, E., Gracia, F., Narayanan, V., Stephen, A., 2015b. ZnO/Ag/CdO nanocomposite for visible light-induced photocatalytic degradation of industrial textile effluents. J. Colloid Interface Sci. https://doi.org/10.1016/j.jcis.2015.04.035.

Saravanan, R., Sacari, E., Gracia, F., Khan, M.M., Mosquera, E., Gupta, V.K., 2016a. Conducting PANI stimulated ZnO system for visible light photocatalytic degradation of coloured dyes. J. Mol. Liq. 221, 1029–1033.

Saravanan, R., Mohammad, M.K., Gracia, F., Qin, J., Gupta, V.K., Arumainathan, S., 2016b. Ce3+-ion-induced visible-light photocatalytic degradation and electrochemical activity of ZnO/CeO2 nanocomposite. Sci. Rep. 6, 31641. https://doi.org/10.1038/srep31641.

Senthil, K.P., Senthamarai, C., Durgadevia, A., 2012. Adsorption kinetics, mechanism, isotherm, and thermodynamic analysis of copper ions onto the surface modified agricultural waste. Environ. Prog. Sustainable Energy 33 (1), 28–37.

Singh, V., Sharma, A.K., Tripathi, D.N., Singh, R., 2009. Poly(methylmethacrylate) grafted chitosan: an efficient adsorbent for anionic azo dyes. J. Hazard. Mater. 161, 955–966.

Sivakumar, B., Kannan, C., Karthikeyan, S., 2012. Preparation and characterization of activated carbon prepared from *balsamodendron caudatum* wood waste through various activation processes. Raysayan J. Chem. 5 (3), 321–327.

Theivarasu, C., Mylsamy, S., 2011. Comparative adsorption study of acid Red 18 on cocoa (*Theobroma cacao)* shell and commercial activated carbon. Int. J. Res. Chem. Environ. 1 (2), 159–165.

Velmurugan, P., Rathina, K.V., Dhinakaran, G., 2011. Dye removal from aqueous solution using low cost adsorbent. Int. J. Environ. Sci. 1 (7), 1492–1503.

Vijayakumar, G., Tamilarasan, R., Dharmendirakumar, M., 2012. Adsorption, kinetic, equilibrium and thermodynamic studies on the removal of basic dye

rhodamine-B from aqueous solution by the use of natural adsorbent perlite. J. Mater. Environ. Sci. 3 (1), 157–170.
Zawani, Z., Luqman, C.A., Choong, T.S., 2009. Equilibrium, kinetics and thermodynamic studies: adsorption of remazol black 5 on the palm kernel shell activated carbon (PKS-AC). Eur. J. Sci. Res. 37 (1), 67–76.
Zazouli, M.A., Balarak, D., Mahdavi, Y., 2014. Application of Canola residuals in absorption of reactive red 198 (RR198) dye from aqueous solutions. J. Neyshabur Univ. Med. Sci. 2, 55–66.